

1 **Distributed Acoustic Sensing (DAS) for Longwall Coal Mines**

2 Derrick Chambers<sup>1\*</sup>, Alexander Ankamah<sup>2</sup>, Ahmad Tourei<sup>3</sup>, Eileen R Martin<sup>3</sup>, Tim Dean, Jeffery Shragge<sup>3</sup>,

3 John A Hole<sup>2</sup>, Rafal Czarny<sup>5</sup>, Gareth Goldswain<sup>5</sup>, Jako du Toit<sup>5</sup>, M Shawn Boltz<sup>1</sup>, James McGuinness<sup>4</sup>

4 1 – National Institute for Occupational Safety and Health, 315 E Montgomery Av. Spokane WA 99207

5 2 – Virginia Tech, 290 College Ave. Blacksburg, VA 2406

6 3 – Colorado School of Mines, 1500 Illinois St, Golden, CO 80401

7 4 – Anglo American, 11/201 Charlotte St, Brisbane City QLD 4000, Australia

8 5 – Institute of Mine Seismology, 10 Church Street, Kingston, Tasmania, 7050, Australia

9 \* – Corresponding author (derchambers@cdc.gov)

10 This manuscript is a non-peer reviewed preprint submitted to EarthArXiv.

11 **Abstract**

12 Seismic monitoring of underground longwall mines can provide valuable information for managing coal  
13 burst risks and understanding the ground response to extraction. However, the underground longwall mine  
14 environment poses major challenges for traditional in-mine microseismic sensors including the restricted  
15 use of electronics due to potentially explosive atmospheres, the need to frequently and quickly relocate  
16 sensors as rapid mining progresses, and source parameter errors associated with complex time-dependent  
17 velocity structure. Distributed acoustic sensing (DAS), a technology that uses rapid laser pulses to measure  
18 strain along fiber optic cables, shows the potential to alleviate these shortcomings and improve seismic  
19 monitoring in coal mines. This work demonstrates several DAS deployment strategies such as deploying  
20 fiber on the mine floor, in boreholes drilled from the surface and from mine level, on the longwall mining  
21 equipment, and wrapped around secondary support cans. This paper also discusses some of the data  
22 processing and deployment improvements that could help DAS-based monitoring become routine in  
23 underground longwall mines. Because DAS applications in coal mines are just now emerging, the findings  
24 presented here will aid decision makers in assessing the potential of DAS to meet their needs and help guide  
25 future DAS deployment designs in underground coal mines.

26

27 **Keywords:** longwall mining; underground coal mining; distributed acoustic sensing; distributed fiber  
28 optic sensing

29

**1 Introduction**

30 Many underground mines experience a variety of dynamic failures that cause violent, near-instantaneous  
31 damage to mine openings. In hardrock mines, these failures are termed “rockbursts,” and though certainly  
32 not a solved problem, significant progress has been made in managing and reducing rockburst risks in the  
33 past several decades [1,2]. A key component of this success has come from improvements in, and increased  
34 adoption of, seismic monitoring. Monitoring seismicity can provide an increased understanding of the earth's  
35 reaction to resource extraction, can be used to forecast seismic hazards to guide mining and ground control  
36 decisions, inform mine re-entry protocols, as well as a variety of other useful functions [3–5].

37 Several studies have demonstrated similar uses of microseismic monitoring in coal mines, which can  
38 also experience violent dynamic failures known as “coal bursts.” Various uses of microseismic monitoring  
39 in coal mines include: detecting fracturing associated with failure of thick strata in the overburden [6] and  
40 water inflows [7]; imaging high stress areas [8]; forecasting bump risk [9]; identifying the activation of  
41 seismogenic geological features [10]; and other useful ground control objectives. Despite an abundance of  
42 promising studies, the coal mining industry has been slow to adopt seismic monitoring. Swanson et al. [11]  
43 highlight some of the challenges that impede longwall mines from routinely operating the same types of in-  
44 mine networks used in hardrock mining, which include: the tendency of coal mines to be much larger and  
45 mine more rapidly than typical hardrock mines; regulations restricting the use of electronics in coal mines  
46 due to potentially explosive atmospheres; and difficulty locating events in the complex, time-varying media  
47 associated with coal extraction in faulted sedimentary environments.

48 Distributed acoustic sensing (DAS), a subset of distributed fiber optic sensing (DFOS) [12], uses rapid  
49 laser pulses to monitor strain and vibration in fiber optic cable. DAS could play a role in making seismic  
50 monitoring in underground coal mines more feasible for the following reasons. First, DAS-compatible cable  
51 is already widely used for data transfer in underground coal mines. Unlike the electronics associated with  
52 traditional seismic systems, these cables pose no risk to initiating an explosion and can be placed anywhere  
53 in a coal mine, provided that the device acquiring the recordings, known as a DAS interrogator unit (IU), is  
54 located in the intake air. Second, because DAS systems can monitor tens of kilometers of cable (hundreds  
55 with some newer systems), monitoring large areas and rapid mining rates becomes much less of an issue

56 than with traditional sensors. Moreover, the densely sensed seismic wavefields recorded underground are  
57 less susceptible to propagation complexity when recordings are taken closer to the source.

58 Published studies have used DAS for monitoring induced seismicity related to hydrocarbon extraction  
59 [13], recording regional and global earthquakes [14], determining seismic site characteristics for earthquake  
60 hazard assessment [15], and several other geophysical applications [16]. A few recent works have  
61 documented DAS deployments in underground mines, such as in the Sanford Underground Research Facility  
62 [17], an active room-and-pillar limestone and dolomite mine [18], and an underground hardrock mine [19].  
63 Examples of DAS deployments in or above coal mines are even more limited. Luo and Duan [20] used DAS  
64 on a cable installed in a borehole and trenched above a mine to monitor caving associated with longwall coal  
65 mining. Chambers and Shragge [21] deployed a DAS-based seismoacoustic array, discussed in **Section 6**,  
66 to monitor coal bursts occurring on the mining face.

67 Each of the aforementioned studies demonstrates the potential of DAS for mining applications. However,  
68 before DAS can become a routine monitoring tool in longwall coal mines, further work is needed to develop  
69 viable deployment strategies as well as data processing and management approaches. This work presents  
70 field trials of several types of DAS deployments in active longwall coal mines and is organized as follows.  
71 First, a review of longwall mining and the relevant concepts to this study, as well as DAS fundamentals for  
72 microseismic monitoring, are reviewed. The following sections describe seven DAS deployments which  
73 included deploying cable on the mine floor, in a vertical and directional borehole drilled from the surface,  
74 in a near-horizontal borehole drilled from mine level, a seismoacoustic array deployed on the longwall face,  
75 fiber deployed in the longwall cable tray, and fiber wrapped around support cans. A discussion of the  
76 strengths and shortcomings of each deployment, as well as the monitoring objectives they could meet, is  
77 then offered. Finally, key challenges and research directions that could help accelerate adoption of DFOS  
78 technology in coal mines are highlighted.

## 79 **2 Background**

### 80 *2.1 Longwall mining*

81 Longwall mining is an efficient, high-extraction mining method for exploiting thin-seam deposits such  
82 as coal, pot ash, and soda ash. Although more capital intensive, the longwall method has yielded significant

83 safety and operational improvements over traditional approaches such as room-and-pillar mining [22]. The  
84 main components of a longwall are a line of shields, a cutting device, and an armored conveyor belt (Fig. 1  
85 a and b). The shields support the roof and provide a protected travel way. They also incrementally advance  
86 as extraction progresses, allowing the roof to cave behind the shield line forming a mined-out zone known  
87 as the gob (or goaf). The cutting device, usually a rotating drum with attached carbide bits known as a  
88 shearer, moves up and down the mining face breaking up the coal and knocking it on the conveyor. The face  
89 conveyor transports the coal to a larger conveyance system so it can be removed from the mine. The cables  
90 that are needed to operate the equipment are attached on the shield side of the conveyor structure or placed  
91 in a cable tray (Fig. 1 b). The power center supplies the high-voltage lines needed to power the longwall and  
92 is typically located several hundred meters ahead of the face. The power center is periodically advanced as  
93 extraction progresses to maintain a safe distance from mining activity.

94 The longwall extracts a rectangular block of coal known as a panel. Typical panel widths (the mining  
95 face dimension) range from 0.2 km to 0.4 km, and panel lengths of 1 km to 4 km are common. The tunnels  
96 on either side of the panel are known as gateroads, with the gateroad adjacent to the previously mined panels  
97 known as the tailgate and the other known as the headgate. The entries are coated with several centimeters  
98 of rockdust, a non-combustible pulverized material, typically limestone, which helps suppress explosions  
99 (Fig. 1 c). Often, longwall mines employ secondary support systems to help maintain the integrity of highly  
100 stressed gateroads, especially the tailgates, to ensure multiple escape routes are traversable and to help the  
101 panel remain properly ventilated. A popular support choice is steel cylinders filled with cement known as  
102 "cans" (Fig. 1 d). A group of adjacent longwall panels separated by gateroads is known as a district. After  
103 all the panels are mined, districts are typically sealed with air-tight barriers after which they are no longer  
104 accessible or ventilated.

105

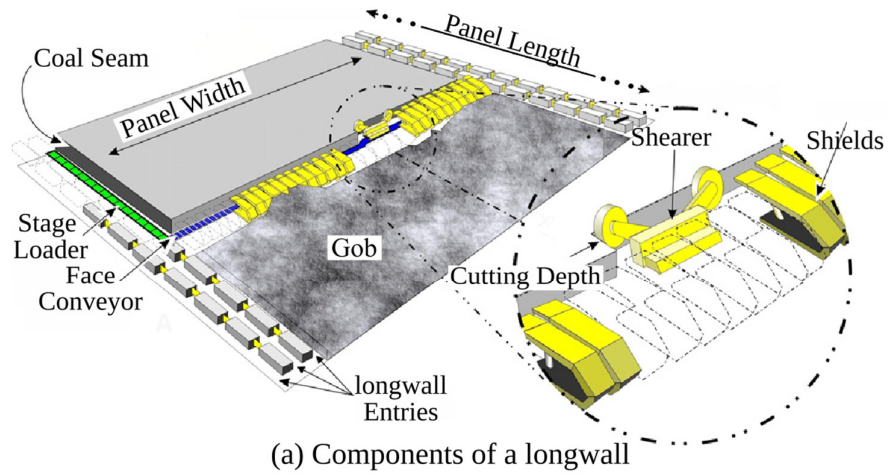


**Fig. 1.** Longwall mining concept. (a) conceptual diagram of the longwall (modified from [23]), (b) A photograph of a longwall face (modified from [24]), (c) A miner applying rockdust in a gateroad (photo in public domain), and (d) installed secondary support cans (modified from [25]).

## 2.2 Distributed Acoustic Sensing

The DAS IU measures strain, strain rate, or less commonly, deformation rate along the fiber optic cable. High sampling rates are supported, easily in the kHz range, but data are often decimated to reduce storage demands. Assuming a homogeneous isotropic medium and long wavelengths relative to the gauge length ( $L$ ), DAS strain rate measurements ( $\dot{\epsilon}$ ) are equivalent to a finite difference of particle velocities ( $\dot{u}$ ), as would be measured by two fiber-aligned geophones separated by  $L$  [26]:

$$\dot{\epsilon}(x, t) = \frac{\dot{u}(x+L/2, t) - \dot{u}(x-L/2, t)}{L} \quad (1)$$

120 For some DAS interrogators,  $L$  (which can be thought of as the length over which strain is averaged) is  
 121 fixed while others allow setting a custom value at acquisition or in post-processing. Compared to traditional  
 122 sensors used in mines, DAS offers a much broader frequency response [27], although the exact performance  
 123 depends on the choice of interrogator and  $L$ . To avoid signal distortions, the smallest apparent wavelength  
 124 of the recorded signal of interest should be several multiples of  $L$ , but smaller values of  $L$  also lead to a lower  
 125 signal-to-noise ratio. This trade-off should be considered in deployment design when an IU with a fixed  
 126 gauge length is used [28].

127 Another aspect that affects the ability of DAS to monitor seismicity is the phase and orientation  
 128 dependent sensitivity, which stems from recording strain rather than particle motion typified in conventional  
 129 geophone sensors [Eq. (1)]. Fig. 2 shows the amplitude factor for in-plane P and SH plane waves for a  
 130 horizontal geophone (a) and a DAS fiber with the same alignment (i.e.,  $0^\circ$ ), assuming the apparent  
 131 wavelength is several multiples of  $L$  (b). Neither sensor directly records SV waves which are polarized out  
 132 of plane. The P-wave sensitivities are similar for both sensor types; however, DAS P-wave sensitivity is  
 133 governed by a  $\cos^2(\phi)$  term, whereas the geophone response is governed by  $\cos(\phi)$ , where  $\phi$  is the ray  
 134 path angle in the X-Y plane measured from the X axis. The S wave sensitivities, however, are significantly  
 135 different. The DAS response is controlled by a  $\frac{1}{2}\sin(2\phi)$  term and the geophone by a  $\sin(\phi)$  term. The  
 136 somewhat surprising result is that DAS is, at least in theory, insensitive to SV plane waves propagating in a  
 137 direction perpendicular to the fiber, whereas the geophone's maximum sensitivity is in exactly this  
 138 orientation. Martin et al. [29] provide further details of DAS sensitivities to surface wave phases,  
 139 directionality, and gauge lengths.

140 One of the simplest methods for locating seismicity recorded by linear DAS cables is to assume that the  
 141 fiber is embedded in a homogeneous, isotropic whole space with a seismic velocity of  $v$ . When the event is  
 142 located within the volume defined by the length of the cable, the observed arrival time ( $t_A$ ) for some distance  
 143 along the fiber ( $x$ ) is related to the event origin time ( $t_0$ ), the shortest distance to the fiber line ( $d$ ), and the  
 144 fiber distance closest to the event ( $x_0$ ) by the following hyperbolic curve:

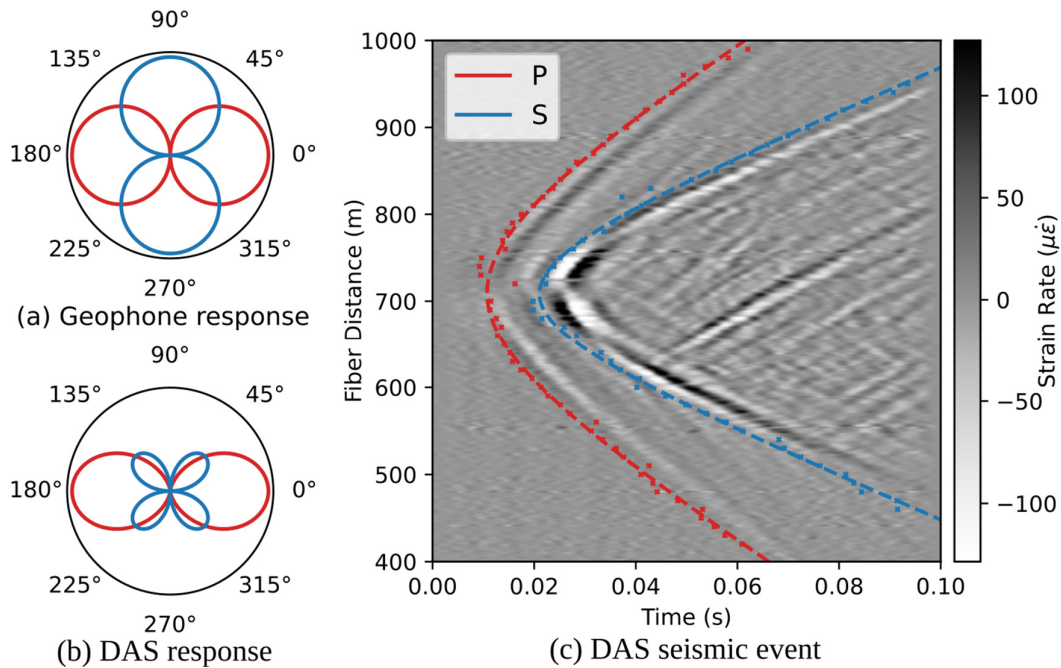
145

$$146 \quad t_A(x) = \frac{\sqrt{d^2 + (x-x_0)^2}}{v} + t_0 \quad (2)$$

147

148 Any of the unknowns in Eq. (2) can be solved using phase arrival estimates and common optimization  
 149 techniques, such as the curve fit implementation in the SciPy library [30]. An important implication of Eq.  
 150 (2) is that the event position in 3D space cannot be determined, only the distance from the fiber and the part  
 151 of the fiber closest to the event can be resolved. This results in a circle of possible event locations around  
 152 the fiber which all fit the data equally well. However, if multiple linear fiber segments (or other seismic  
 153 sensors) are available and favorably oriented in relation to a seismic event, absolute locations can be  
 154 constrained [31].

155



156

157 **Fig. 2.** (a) Sensitivity to P (red) and S (blue) waves for a geophone and (b) the sensitivity for a linear DAS  
 158 fiber oriented along the X axis (0 degrees), assuming apparent wavelengths that are several multiples of the  
 159 gauge length [32]. (c) An example of fitting Eq. (2) (dotted lines) to manual phase picks (dots) in order to  
 160 estimate the location of a seismic event recorded by fiber in a borehole [33].

161

### 3 Gateroad Deployment

162 In-mine sensors close to seismic events are valuable for optimizing location accuracy and network  
 163 sensitivity. Typically, accelerometers or geophones are installed in several shallow boreholes drilled from  
 164 the mine workings. However, it may be possible to gain similar benefits from the dense recordings of a DAS

165 cable distributed throughout the mine workings. To test this type of deployment, a fiber optic cable was  
166 installed in a deep US coal mine which has a history of problematic seismicity caused by thick competent  
167 strata (TCS) failing in the overburden [34]. The DAS IU was placed in a climate-controlled shelter at the top  
168 of a ventilation shaft. Several fiber optic cables were connected from the shaft, through the mains, and to the  
169 active panel with a total fiber length of approximately 7 km. Due to access restrictions, and to be able to  
170 monitor both the headgate and tailgate with a single IU, a single cable was placed in the headgate and two  
171 fibers in the same cable were spliced together at the end to allow optical signals to travel down and back the  
172 entire length of the cable (Fig. 3 a). A 1,280-m section of the cable was placed on the floor and covered with  
173 rockdust (Fig. 1 c), where available, to improve coupling [35], which demonstrably provided a better signal  
174 than fiber zip-tied to the roof, ribs, or hung from cable hooks. Unfortunately, a faulty splice connecting the  
175 headgate cable to the tailgate cable made the tailgate fiber unusable for recording event waveforms.

176 During the 47 days of recording, many events with varying magnitudes were visible in the raw  
177 (unfiltered) DAS data (Fig. 3 b and c). For the largest magnitude event recorded during the deployment  
178 (referred to as event 1,  $M = 1.2$ ), the simple procedure described in **Section 1** applied to P-wave arrivals  
179 indicates a distance from the closest point on the cable ( $d$ ), the center channel distance ( $x_0$ ), and velocity ( $v$ )  
180 of  $d = 0.45$  km,  $x_0 = 0.9$  km,  $v = 4.8$  km/s. The estimate of  $d$  is close to the horizontal distance of  
181 approximately 0.41 m estimated from a catalog created with data from a surface seismic network. The  
182 location discrepancy could be rectified if the event occurred some distance into the roof and is acceptable  
183 considering that horizontal errors of a few tens of meters are typical for locations derived from surface  
184 networks. For a much smaller event occurring on the headgate side of the panel (example event 2,  $M =$   
185  $-0.3$ ) phases are also clearly visible (Fig. 3 c) and the hyperbolic curve fit yields  $d = 0.09$ km,  $x_0 =$   
186  $0.63$  km,  $v = 4.7$  km/s.

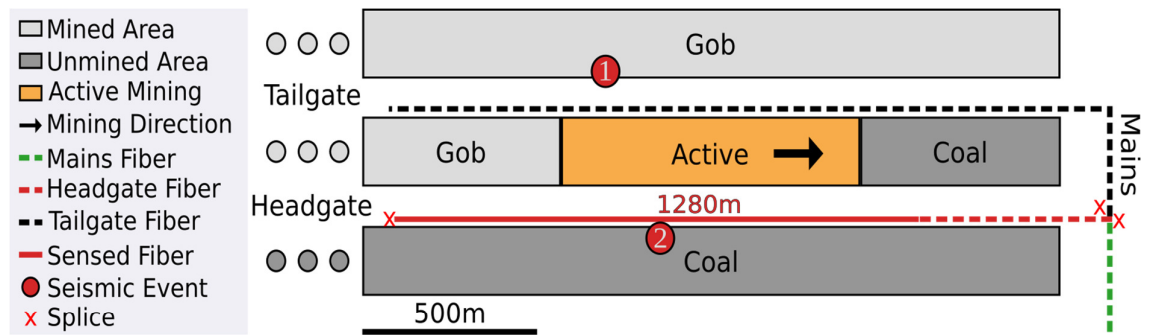
187

188

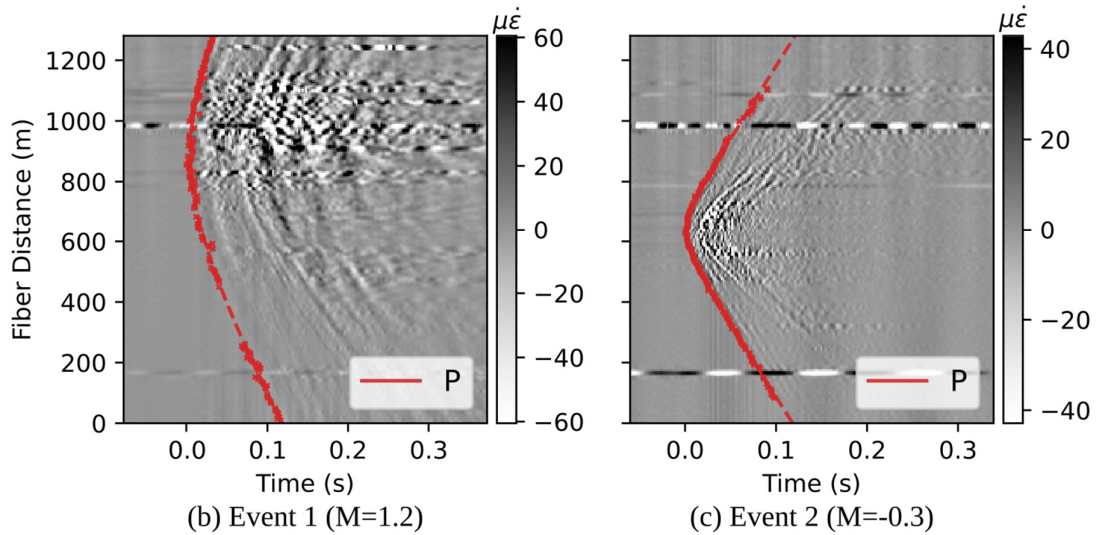
189

190





(a) Deployment map



(b) Event 1 ( $M=1.2$ )

(c) Event 2 ( $M=-0.3$ )

**Fig. 3.** Gateroad deployment and example data. (a) A simplified version of the deployment geometry, truncated panel outlines, the area mined during the deployment, and several other features; (b) The unfiltered strain-rate DAS data for example event 1 located on the tailgate side of the active panel ( $M = 1.2$ ) as well as P-phase picks and a hyperbolic best-fit curve (dashed line); (c) shows the same as (b) but for example event 2 ( $M = -0.3$ ) located on the headgate side of the active panel.

191

192

193

194

195

196

197

198

199

200

201

202

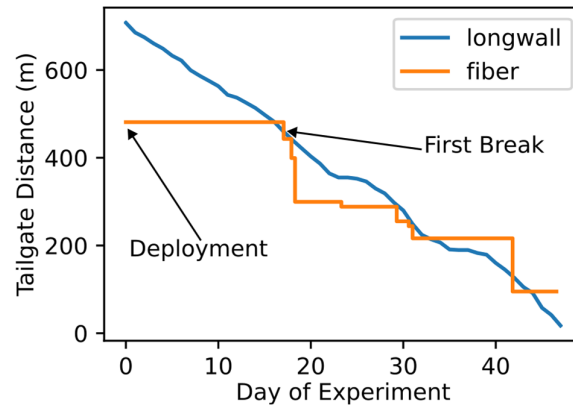


**Fig. 4.** Relative position of the longwall (blue) and tailgate fiber end (orange) with discrete fiber breaks represented by vertical segments in the orange line.

There are several challenges associated with gateroad deployments, namely the need for multiple splices which can compromise the fiber, the susceptibility of the cable to caving or operations-related damage, and potentially lower sensitivity due to less-than-ideal coupling and the rugosity of the damaged excavation surface on which the cable rests. Although du Toit et al. [35] found that fiber tied to mesh was of limited use for recording small ( $M < 0$ ) seismic events in a hardrock mine, Fig. 3 demonstrates that fiber deployed on the mine floor and covered with rockdust is useful for detecting and locating both larger events ( $M > 1$ ) several hundred meters from the fiber and smaller events ( $M < 0$ ) originating closer to the fiber.

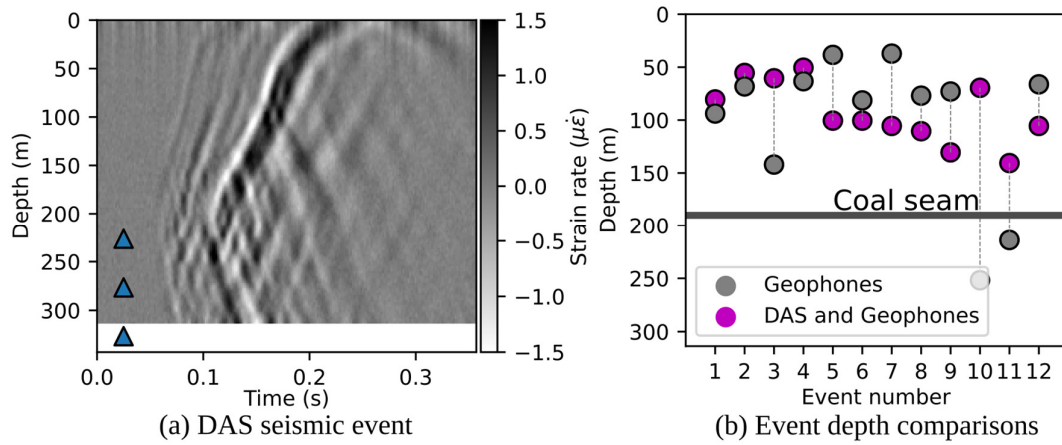
While some progress has been made on this dataset, additional work is needed to develop and refine pre-processing workflows to improve signal-to-noise ratios of body wave phases. Additionally, determining best practices to optimize cable survival, which may simply involve appropriate cable selection and deployment locations which will not interfere with operations, will be important before mines can routinely and robustly use this deployment strategy. Moreover, if durable fiber can be distributed throughout the mine gateroads, it could not only match or exceed the event detection and location capabilities of traditional in-mine microseismic systems, but may also be useful for other DFOS-related safety applications such as detecting thermal events in mined-out areas [36].

#### 4 Surface Borehole Deployment

223       When seismic sensors are installed from mine workings in a single seam, or exclusively on the surface,  
224 accurately estimating the depths of seismic events is challenging because the sensor geometry is nearly  
225 planar. To address this limitation, seismic sensors can be positioned both near the seam and on the surface  
226 and/or in a borehole [37]. DAS shows promise to densely probe the seismic wavefield in horizontally  
227 stratified layers typically found in coal mines. This section presents two examples of DAS deployments  
228 which help constrain the vertical coordinates of seismic events in the vicinity of underground coal  
229 exploitation.

230       The first example shows a fiber optic cable grouted in a vertical borehole drilled from the surface over a  
231 gateroad of an active panel. The DAS data and geophones installed in the same borehole were used to locate  
232 induced seismicity. Fig. 5 (a) shows an event recorded by this configuration. In this case, a more  
233 sophisticated location scheme than the one presented in **Section 2.2** was employed. The DAS strain-rate data  
234 were transformed into a probability grid using matched field processing techniques [38]. The grid served as  
235 a prior in the location algorithm, which incorporated P- and S-wave first arrivals from the geophones to  
236 better vertically constrain the event depth (Fig. 5 b). We apply this workflow to a set of events, all of which  
237 shift above the seam from their original locations determined with only geophone data. Their vertical  
238 locations correspond to DAS waveforms that focus within the strata above the seam. Using only a sparse  
239 geophone array leads to a mirroring effect, i.e., locations above and below the seam can result in similar  
240 residuals in the location.

241



242

243

244

245

246

247

248

249

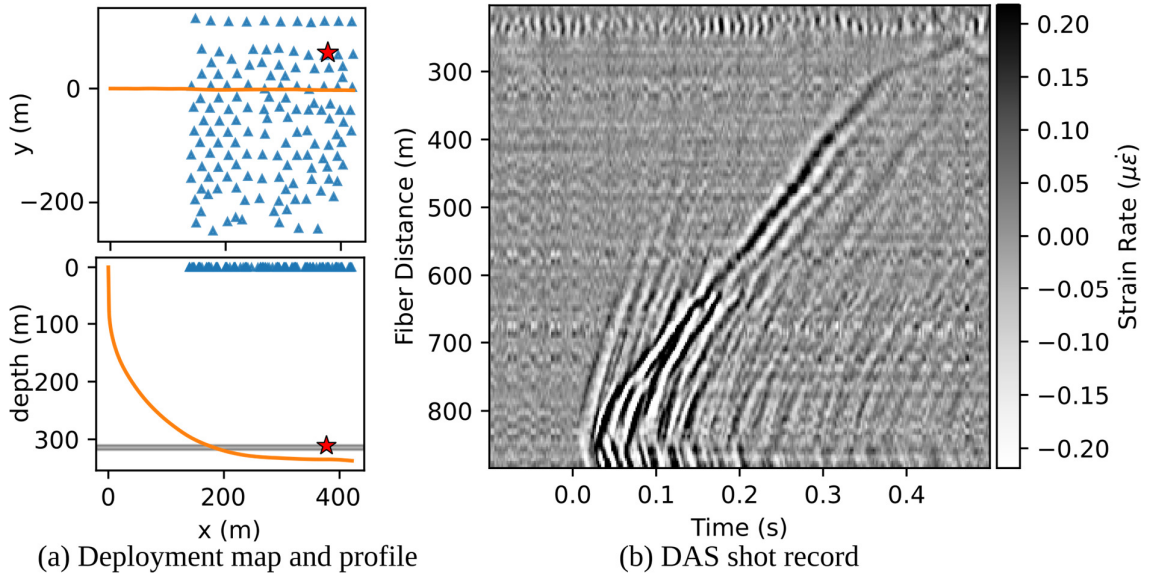
250

251

252

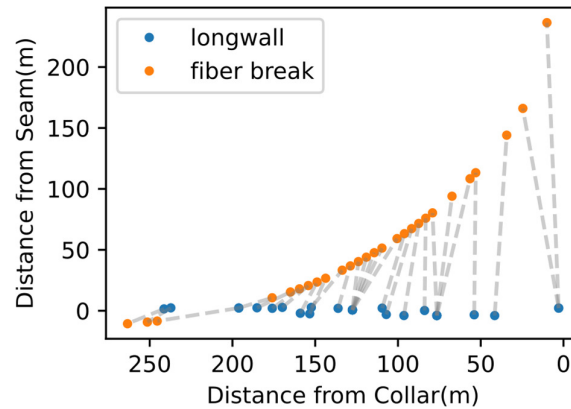
- **Fig. 5.** Vertical borehole DAS data. (a) An example event recorded on a fiber in a vertical borehole. The blue triangles indicate the depths of the tri-axial geophones in the borehole with the fiber. (b) Changes in event locations using only geophone data and including DAS data.

In the second example, a fiber cable was grouted into a directional borehole drilled from the surface and over 100 nodes (portable, self-contained geophone stations [39]) were deployed on the surface (Fig. 6 a). The goals of the experiment were to explore the utility of the DAS data in locating and understanding seismicity, and to assess and calibrate an event location procedure using the node data. To that end, a small calibration blast was detonated from the coal seam which was recorded clearly in the DAS data (Fig. 6 b).



253 (a) Deployment map and profile  
 254 **Fig. 6.** Directional borehole DAS data. (a) Deployment map (top) and profile view (bottom) where the blue  
 255 triangles are the surface nodes, the red star indicates the location of a calibration blast, the orange line is the  
 256 fiber, and the gray horizontal bar indicates the location of the coal seam. (b) DAS recording of a calibration  
 257 blast.

258  
 259 These two examples demonstrate that DAS deployments in surface boreholes can provide a clear picture  
 260 of event-induced strain fields which can help improve event location estimates, particularly in depth. The  
 261 borehole cable also has the advantage of being isolated from mine operations, which reduces noise  
 262 contamination and risk of damage associated with operating equipment. However, in both cases, extraction-  
 263 induced ground motions were severe, and the cable was sheared several times as the longwall advanced. For  
 264 example, [Fig. 7](#) shows the position of the longwall as various breaks occurred in the DAS cable. Other  
 265 disadvantages of this deployment type include the requirements of a borehole and infrastructure for  
 266 protecting, powering, and communicating with the DAS IU. Of course, these disadvantages are mitigated if  
 267 suitably located boreholes already exist (e.g., exploration or degassing holes) and surface infrastructure or  
 268 fiber lines to other structures are readily available. Moreover, vertical wells instrumented with DAS fiber  
 269 are useful in vertical seismic profiling (VSP [40]), which could be used to build a velocity model for other  
 270 surface-based seismic deployments or to monitor time-dependent changes in the near-fiber geological  
 271 structure.



273

274

**Fig. 7.** Horizontal and vertical position of the longwall and associated fiber breaks in the directional borehole. All but 2 of the 28 breaks occurred between 30m behind and 30m ahead of the longwall.

275

276

277

## 5 In-mine Borehole Deployment

278

279

280

281

282

283

284

285

286

287

288

289

290

291

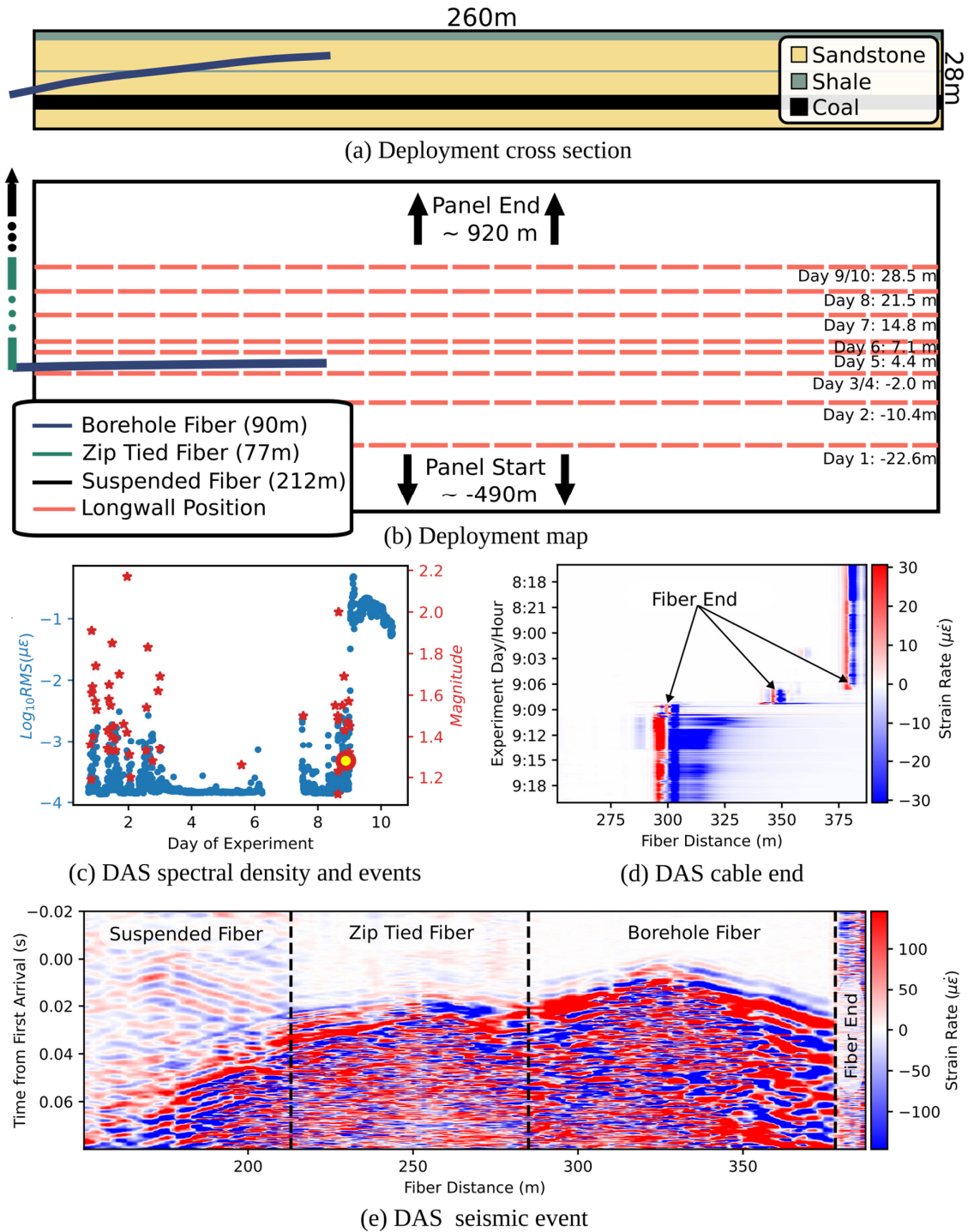
292

293

DAS can also be deployed in boreholes drilled from the mine level. One objective of such a deployment is to monitor the mechanical behavior of undermined massive strata which can cause myriad ground control issues if proper caving is not achieved [41]. In this experiment a DAS cable was installed in a near-horizontal borehole drilled from mine level into a thick competent sandstone (Fig. 8 a and b). The mine experienced coal bursts on the mining face (i.e., face bursts) with contributing factors being thickness and strength of the near-seam TCS, high-strength brittle coal, significant depth of cover (0.65 km), and a seam dip greater than 12° [41]. The DAS IU was located at the longwall's power center several hundred meters from the mining face. The cable included three coupling configurations involving fiber: suspended from the roof by cable hooks, zip-tied to metal mesh on the roof, and inserted into the borehole. The fiber was inserted by attaching it to threaded sections of polyvinyl chloride (PVC) rods and manually pushing the rods into the hole. Unlike the deployments detailed in **Section 4**, the fiber was not grouted in the borehole which certainly resulted in lower fidelity measurements of rock strain.

The experiment lasted for about 10 days as the longwall advanced from approximately 20 m behind the borehole to 20 m ahead of it. During the deployment, a regional seismic network located 50 events near the mining area which ranged in magnitude from 1.1 to 2.2 (Fig. 8 c). A temporary increase in the background noise level of the borehole fiber was observed when the shearer was operating and a permanent increase (on

294 day 9) as the cable sustained damaged due to large deformations in the TCS. These phenomena are easily  
295 observed by averaging the root mean square (RMS) strain rate of all borehole channels for two minute  
296 increments (Fig. 8 c). Locations and times of breaks in the fiber, and presumably the surrounding rock, were  
297 identified by first low-pass filtering, decimating, and concatenating many hours of DAS data. The filter-  
298 induced Gibbs effects at the end of the cable define the farthest point the fiber remains able to transmit light  
299 (Fig. 8 d). Interestingly, both the borehole and zip-tied fiber acquired high-amplitude signals with  
300 identifiable apices for events occurring on the headgate side of the panel (Fig. 8 e).



301

302 **Fig. 8.** In-mine near-horizontal borehole fiber deployment. (a) Cross section of the near-seam geology and

303 the location of the sensing fiber (blue line). (b) Map view of the deployment with three types of fiber and

304 longwall positions as a function of experiment duration. (c) Seismic events detected by a regional network (red)

305 as well as the logarithm of the average root mean square strain rate for every two minutes of DAS data (blue).



306 (d) Changes in the end of the cable which broke in two segments over the course of a few hours on day 9. (e)

307 Example data of a \$M 1.3\$ event, the red dot with yellow center in (c), on the three types of fiber.

308

309 This type of deployment could provide several types of useful geomechanical information. First, the  
310 mechanisms of coal bursts are not well understood and vary from mine to mine. For example, some of the  
311 proposed face bursts' mechanisms involve a sudden failure of TCS above the gob which then causes a rapid  
312 redistribution of stress on the face, while others propose that the primary failure occurs entirely in or near  
313 the coal seam without any significant dynamic contribution of the TCS [42,43]. Direct measurements in the  
314 TCS as these failures occur could shed additional light on these physical processes, which, in turn, could  
315 enable more informed, site-specific, coal burst mitigation strategies. Second, it may be possible to  
316 characterize crack initiation damage stress thresholds by identifying and tracking acoustic emissions  
317 occurring near the fiber, perhaps similar to the laboratory procedure outlined by Zafar et al. [44]. Third,  
318 interferometric techniques [45] may be able to identify time-dependent seismic velocity or attenuation  
319 changes indicative of progressive TCS failure.

320 The main disadvantage of this type of deployment is the need to drill a horizontal borehole from seam  
321 level, which can be labor intensive and costly. The sub-optimal coupling of the fiber in our case could also  
322 be an issue as grouting the fiber in place would provide better rock strain signals. However, leaving the cable  
323 ungrouted also allows it to slip as the TCS undergoes large strains and thereby enabling the collection of  
324 more data before the fiber fails.

325

## 326 **6 Longwall Face Deployments**

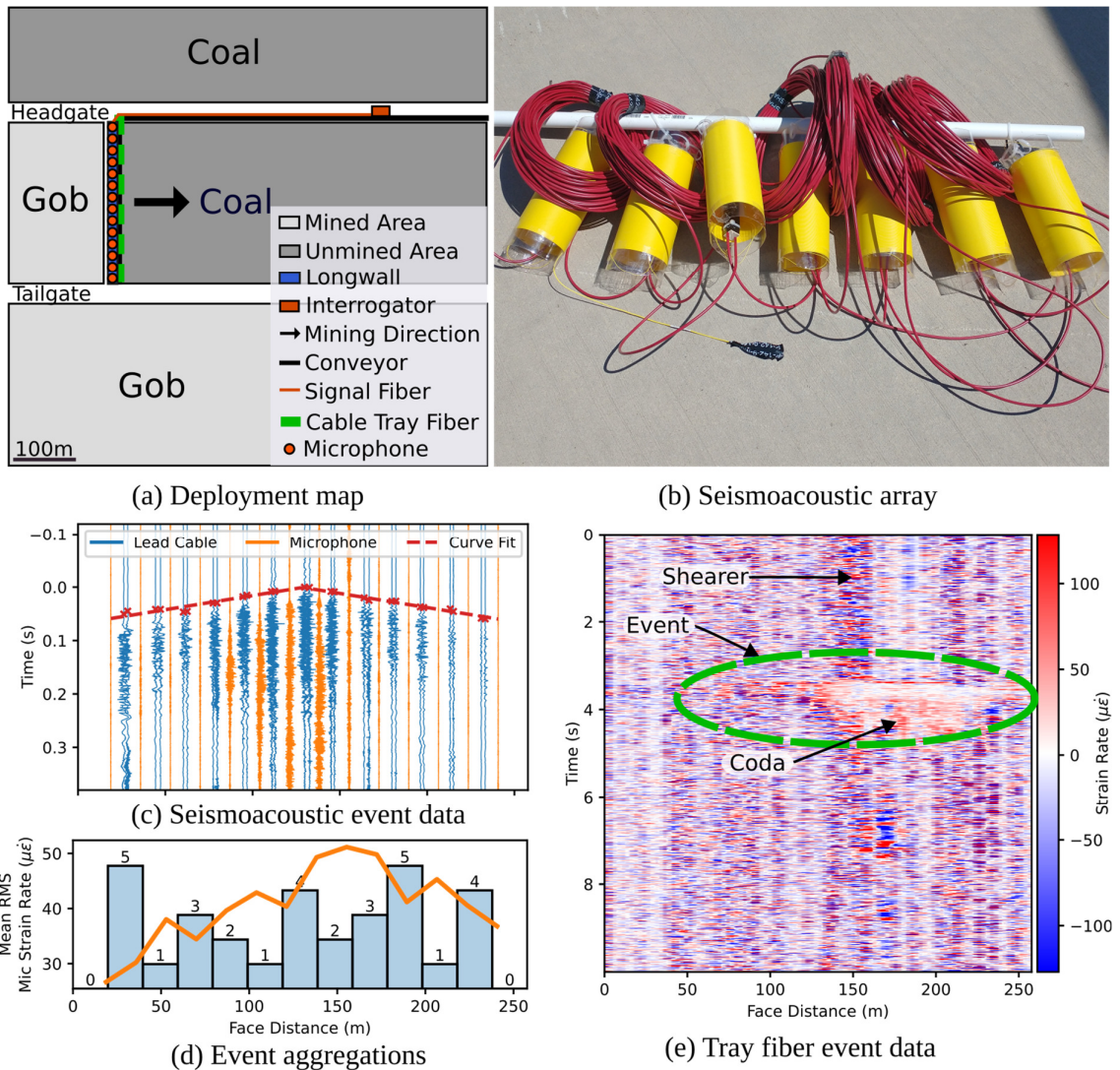
327 Another intriguing possibility for DAS is to monitor areas of the mine that would be largely impractical  
328 to deploy traditional sensors, such as on the longwall face itself. This would be particularly useful when face  
329 bursting is a known hazard. This section details two experiments in the same mine mentioned in **Section 5**  
330 which experienced face bursts (Fig. 9 a). Chambers and Shragge [45] describe the first deployment which  
331 utilized a new kind of seismoacoustic array (Fig. 9 b) composed of two fiber configurations: "lead cables"  
332 and "microphones." The lead cables were standard tight-buffered signal cable fastened to the hydraulic hoses

333 connecting the longwall shields. The second configuration consisted of fiber optic microphones which were  
334 thin-walled plastic cylinders wrapped with 90 m of tight-buffered fiber, resulting in a solid yellow  
335 appearance. The microphones measured air pressure converted to fiber strain in the cylinder, thus allowing  
336 sounds in the audible range to be recorded. For the second deployment, a cable was simply inserted into the  
337 cable tray (Fig. 1 b). In both deployments the DAS IU was co-located with the longwall's power station  
338 about 400 m from the face on the headgate side of the panel.

339 The lead cables of the seismoacoustic array recorded the vibrations excited by the face bursts' elastic  
340 wavefield, and the microphones recorded the burst-related sound waves propagating in the workings.  
341 Examples of both types of waveforms recorded by the array for a  $M = 1.8$  face burst, as well as the first-  
342 arrival picks and the best fit hyperbolic curve, are shown in Fig. 9 c, using Eq. (2) and the optimization  
343 scheme already described,  $d = 0\text{~m}$ ,  $x_0 = 130\text{ m}$ ,  $v = 1.9\text{ km/s}$ . Considering about 30 face bursts over  
344 several shifts, the lead cable waveforms tended to be impulsive, meaning estimating phase arrival times is  
345 feasible and are useful for identifying the event apex which coincides with  $d$ . The microphone channels are  
346 more emergent and could be used for quantifying damage location and severity. For example, Fig. 9 d shows  
347 the binned apex location for the events, as well as the microphone root mean square (RMS) strain rate, a  
348 proxy for acoustic energy, as a function of face distance. The maximum microphone RMS occurs between  
349 the center of the panel and the tailgate, which, anecdotally, coincides with the most severe face bursts for  
350 this panel. The events with apices on the edge of the array might not have occurred on the mining face.

351 Unfortunately, the data from the cable tray deployment were less usable. Although the events were  
352 clearly visible, as well as the location of the shearer before the event (Fig. 9 e), the background noise levels  
353 were too high to make accurate arrival time picks even after applying a variety of common filtering  
354 techniques. The event coda location and duration, however, likely coincide with the settling of ejected coal  
355 and therefore might be used as a proxy for burst damage. Moreover, with more advanced filtering and noise  
356 suppression, the signals may become usable.

357



358

359

360

361

362

363

364

365

366

367

368

**Fig. 9.** Longwall face deployments. (a) Deployment geometry map. (b) Part of the seismoacoustic array consisting of lead cables (red) and microphones (yellow). (c) Waveforms from the lead cable (blue) and microphone (orange) from a  $M = 1.8$  face burst. The first-arrival picks (red Xs) and the best-fit hyperbolic curve (dashed red line) are also shown. (d) The binned apex locations determined from the lead cable channels (blue bars) and the average microphone RMS acoustic strain rate (orange line) for 1.0 s of data after the first arrival for the 30 face bursts recorded by the seismoacoustic array. (e) Example data from the cable tray deployment recording a different  $M = 1.8$  face burst.

The deployments detailed in this section could be useful in addressing face burst risks by providing quantitative data on face burst location and severity (acoustic power or coda duration). These measures in

369 turn could guide tactical and strategic efforts to mitigate related risks. They also have the huge advantage of  
370 rarely needing reconfiguration; the sensors move with the mining face and the IU could be relocated at the  
371 same time as the substation, requiring very little routine maintenance provided the cables on the longwall  
372 remain intact.

373 These longwall-centered deployment strategies on their own, however, would be much less useful for  
374 monitoring other types of seismicity, such as events occurring in overburden strata or gateroad pillars. Also,  
375 because the array is located so close to the mining equipment, it will be much less sensitive than fiber  
376 deployed in quieter sections of the mine. Because the cable is not directly coupled to the rock, and there will  
377 be complex geometries and equipment interactions, it would be extremely difficult to ascertain anything  
378 beyond basic kinematics of the strain field propagating in rock from these data. Moreover, the uncertain  
379 coupling and shifting geometry make identifying which seismic phases the array records challenging, and  
380 since the array is so close to the source, near field phases are likely [46].

381

382

## 7 Support Can Deployment

383 As mentioned in **Section 2.1**, cement-filled steel cans (Fig. 1 d) are commonly used for secondary  
384 support. As the cans take weight from the roof and floor converging, micro-cracks associated with the  
385 excavation damage are forced closed and unconsolidated materials under and above the cans are compacted.  
386 This allows for efficient transmission of elastic waves through the cans, which could be measured by  
387 wrapping them with fiber. This type of deployment might complement deploying cable on the mine floor or  
388 ribs which can experience significant free-surface amplifications and "ringing" due to poor rock coupling.  
389 Unlike cable deployed on the floor, the can dilation is sensitive to vertical strain, providing an additional  
390 direction of strain-field sampling. Moreover, as quasi-static loading progresses, the circumference of the  
391 cans increases due to Poisson's effect. Measuring the long-term changes in circumferential strain may be  
392 useful for understanding extraction-related stress redistribution. Low-frequency DAS processing, which has  
393 been used for several years in the oil and gas industry [47] and for monitoring enhanced geothermal systems  
394 [48], may be able to provide such measurements.

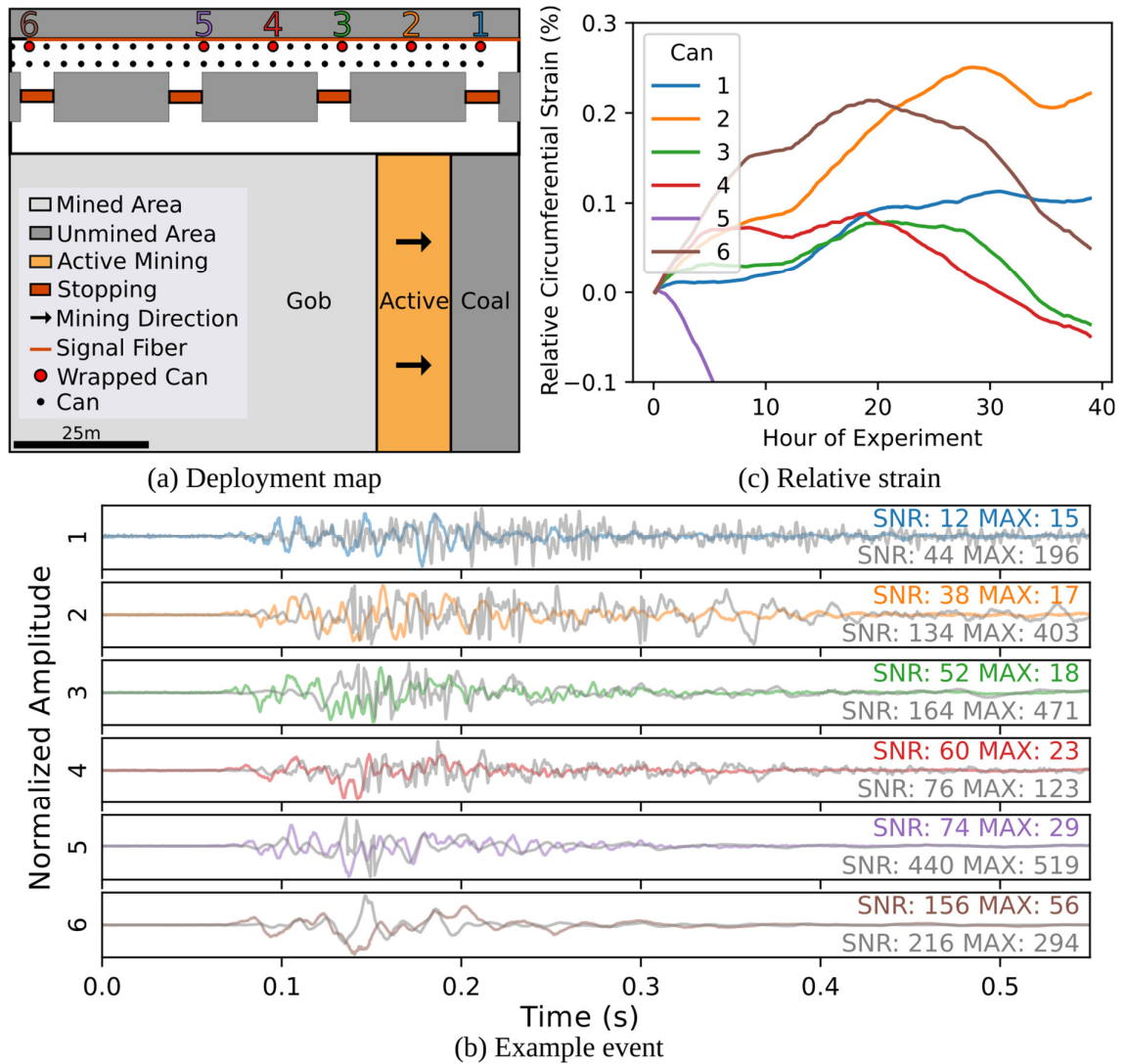
395 To test these theories, 6 different support cans were tightly wrapped with approximately 20 m of fiber in  
396 the headgate of an active longwall mine (Fig. 10 a). The cans were spaced 3 m apart, had a height of 3 m,  
397 and a diameter of 0.6 m. Between the cans, cable was deployed on the gateroad floor in the same fashion  
398 mentioned in Section 3. Composite strain rate time series were created for each can by first removing a  
399 nearly constant strain rate mean of  $1.1 \mu\epsilon$  from all channels, then averaging the center 12 m of strain  
400 recordings of each can. Data from fiber that might be close to the end of the wrap was not used to avoid  
401 including any cable that might be sensitive to non-can strain. For larger events ( $M > 1$ ), the unfiltered floor  
402 strain rate channels had 1 to 6 times higher signal-to-noise ratios (SNR), and 5 to 20 times higher amplitudes  
403 compared to the can signals recorded in the same vicinity (Fig. 10 b). The can signals, however, tend to have  
404 more impulsive first arrivals.

405 To estimate change in can circumferential strain over the duration of the experiment, a 5-second moving  
406 window average was applied to every second of can strain-rate data. The moving average operator acts as a  
407 low-pass, smoothing, and decimation operation and is more efficient than applying these steps sequentially.  
408 The strain-rate data were then integrated along the time axis to yield an estimate of change in circumferential  
409 strain for the approximately 40-hour experiment duration (Fig. 10 c). The two cans subjected to a front  
410 abutment load during much of the experiment (cans 1 and 2) experienced an overall dilation, whereas cans  
411 3 and 4 experienced an increase before decreasing to less than their initial values. The behavior of the first  
412 four cans is consistent with an advancing forward-abutment load which gradually decreased as the longwall  
413 distances increased. Can 5 exhibited a near constant decrease to a final strain of about -0.3% and can 6  
414 experienced a significant increase before returning to nearly the same level as at the start of the experiment.

415 The decreases in relative strain, especially the drastic behavior of can 5, should be interpreted cautiously.  
416 It could be that the fiber simply began to slacken, sliding past the can surface rather than reflecting changes  
417 to the can shape. Certainly, more experience with this type of deployment is needed before we can determine  
418 how robustly DAS is able to measure can strain, and validation with common instruments such as borehole  
419 pressure cells inserted into the coal or pressure plates placed between the can and roof would be a prudent  
420 next step. A Brillouin-based distributed strain sensing (DSS) system could also interrogate a different fiber  
421 in the same cable to get a more direct static strain measurement.

422

423



424

425 **Fig. 10.** Can Deployment. (a) Deployment map showing wrapped cans (labeled 1-6). The DAS IU is located  
 426 several hundred meters to the right of the mining face. (b) Example event ( $M = 1.5$ ) recorded by the can loops  
 427 (colored) and nearest fiber deployed on the mine floor (grey) where each signal has been detrended and  
 428 normalized to its maximum value. The signal-to-noise ratios (SNR) and maximum signal amplitudes (MAX) are  
 429 listed in each plot. (c) Low-frequency can strain from DAS data. Can 5 decreases nearly monotonically to a  
 430 minimum strain of approximately -0.003 but the whole plot is not shown as to avoid obscuring detail of the  
 431 other cans.

432

**8 Discussion**

433

434 *8.1 Additional DAS Advantages for Longwall Coal Mines*

435 In addition to long sensing length, potential to deploy fiber in return air, and near-source recordings, a  
436 few other benefits of DAS to longwall mines are worth mentioning. First, most mines already have extensive  
437 experience with fiber optic installations for communications, much of which is transferable to DFOS  
438 applications. In a practical sense, this means mine personnel could deploy fiber, repair fiber breaks, and  
439 connect sensing segments into existing infrastructure without much additional training. All measurements  
440 of a single IU are naturally time-synchronized which simplifies the complexity of temporally synchronizing  
441 underground equipment as is required for traditional in-mine seismic networks.

442 Because spatially dense DAS recordings contain more wavefield information than sparse point sensors,  
443 they have some significant advantages. First, it is much easier to identify seismic phases based on their  
444 apparent velocity which makes arrival time estimation easier and reduces the risk of mislabeling phases.  
445 Second, more signal processing routines are available for dense spatially sampled data, such as F-K filtering,  
446 which can remove signals with non-seismic propagation speeds. Finally, the wave propagation information  
447 in the DAS records could alleviate the need for frequent calibration blasts as velocity estimations can be  
448 made from the recorded data (e.g., [Fig. 2 c](#), [Fig. 3 b and c](#), [Fig. 6 b](#)). Typical active source exploration  
449 workflows may work well with these data.

450 *8.2 Challenges and Opportunities*

451 Of course, DAS has some disadvantages and barriers to adoption in coal mines. First, because it is a relatively  
452 new approach to passive seismic monitoring, several data processing areas are not yet mature. These include  
453 dealing with variable ground coupling quality and estimating source parameters such as event magnitude,  
454 energy, and moment tensors from DAS data. In the short term, a pragmatic approach to overcome these  
455 challenges is the use of hybrid networks so that data from sparse, in-mine, or surface stations can provide  
456 reliable source parameter estimates, while dense DAS data improve event locations and help quantify local  
457 propagation effects. Second, DAS IUs are still relatively expensive, typically ranging from 100,000 USD to  
458 250,000 USD. Unless a mine experiences damaging seismic events, this level of investment may be difficult

459 to justify. Third, most mine sites are unprepared, in terms of experience and computation infrastructure, to  
460 handle the large volumes of data a DAS IU can produce, which can reach several Terabytes per day. The use  
461 of emerging machine learning tools and specialized open-source software [49] for analysis of DAS data may  
462 help overcome these challenges. Finally, many of the strategies outlined in this paper require significant  
463 design improvements to survive long-term in the rugged mining environment.

### 464 8.3 *Practical Deployment Lessons*

465 Several important lessons were learned from the field deployments. First, apart from the cable being  
466 damaged by mining equipment, splices are the most likely failure point in a fiber array and therefore should  
467 always be properly protected such as in a splice tray or outdoor-rated splice protector. Second, an optical  
468 time domain reflectometer (OTDR) trace is much better for assessing splice quality than the estimate  
469 provided by a fusion splicer. Third, one can reduce data loss risk by ordering the sections of fiber so that  
470 only the later fiber segments are in the areas more likely to collapse or come into contact with machinery.  
471 Fourth, when connecting sensing cable to mine fiber infrastructure, even "obviously true" assumptions about  
472 the fiber system should be verified. For example, during the experiment in **Section 3** several hours were  
473 wasted tracking down a previously undocumented splice which connected fibers of different colors between  
474 the top of the ventilation shaft and the bottom. Lastly, the proper interrogator configuration can make the  
475 difference between recording high-quality strain signals or exclusively instrument noise. Consulting with  
476 the DAS manufacturer and bringing reference configuration documentation to the field are prudent measures.

### 477 8.4 *Future Work*

478 In the opinion of the authors, there are several important research steps needed to accelerate routine DAS  
479 monitoring in longwall coal mines. First and foremost, is to continue to collect DAS coal mine deployments  
480 and improve data processing methodologies. Perhaps the first step in this direction is to move beyond  
481 processing paradigms which either require overly simplified velocity models (as was used here) or neglect  
482 to take advantage of the strong spatial relationships inherent in DAS data by treating each DAS channel as  
483 an independent measurement. The spatial relationships between channels can help in filtering, arrival time  
484 estimation, phase association, etc. and ultimately provide many advantages over traditional networks.



485

486 For non-borehole deployments, comprehensive field research on cable survival and sensitivity is needed.  
487 Deploying various cable types in different configurations (e.g., trenched, laying on the surface, in tight  
488 conduit, etc.) nearly collocated in gateroad floors then continuously monitoring static and dynamic strains  
489 as mining progresses would provide valuable information that might lead to general recommendations and  
490 standard deployment practices. For example, the static strain distribution on each configuration will provide  
491 insight into failure locations and modes, and the dynamic strain of common events can be used to make  
492 sensitivity comparisons.

493

## 9 Conclusions

494 This study details several DAS deployment strategies that show potential to meet various ground-control  
495 objectives in underground longwall coal mines. This includes monitoring routine seismicity occurring in the  
496 gateroads and overburden, quantifying damage from coal bursts occurring on the longwall face, observing  
497 geomechanical behavior of undermined strata, and monitoring static and dynamic stress on secondary  
498 support systems. These nascent fiber optic sensing applications will require additional research and  
499 development to improve both data processing and deployment robustness before they can be used routinely  
500 in underground mines. Nonetheless, the underground coal mining industry stands to gain significant benefits  
501 from DAS technology.

502

## 10 Acknowledgements

503 We would like to thank various mining operations for allowing us to conduct DAS research in their  
504 mines and for providing other forms of support. We would also like to thank Terra15 for answering our  
505 questions and providing technical support for many of these experiments. We would also like to thank the  
506 following people who helped in planning or implementing at least one of the deployments: Jim Garner, Will  
507 Ray, Matthew Tascione, Frantisek Stanek, Dhari Alharbi, Sean Bemis, Amna Alashkhari, Karen Williams,  
508 Erik Westman, Martin Chapman, and Gabriel Walton. We also thank Virginia Tech Advanced Research  
509 Computing for resources. We found the DASCore python package [49] useful for data processing. This  
510 research was supported in part through the NSF IUCRC Center to Advance the Science of Exploration to

511 Reclamation in Mining. The findings and conclusions in this report are those of the author(s) and do not  
512 necessarily represent the official position of the National Institute for Occupational Safety and Health,  
513 Centers for Disease Control and Prevention or any other employer of the listed authors. Mention of any  
514 company or product does not constitute endorsement by NIOSH, CDC. The authors declare they are free of  
515 competing interests.  
516

517

**11 References**

518 [1] Durrheim RJ. Mitigating the risk of rockbursts in the deep hard rock mines of South Africa: 100  
519 years of research. *Extracting the Science: A Century of Mining Research*, Brune J (Eds), Society for Mining,  
520 Metallurgy, and Exploration, Inc 2010:156–71.

521 [2] Simser BP. Rockburst management in Canadian hard rock mines. *Journal of Rock Mechanics and*  
522 *Geotechnical Engineering* 2019;11:1036–43.

523 [3] Potvin Y. Strategies and tactics to control seismic risks in mines. *Journal of the Southern African*  
524 *Institute of Mining and Metallurgy* 2009;109:177–86.

525 [4] Mendecki AJ, Lynch RA, Malovichko DA. Routine micro-seismic monitoring in mines. *Australian*  
526 *Earthquake Engineering Society 2010 Conference*, 2010, p. 1–33.

527 [5] Hudyma M, Potvin YH. An Engineering Approach to Seismic Risk Management in Hardrock  
528 Mines. *Rock Mech Rock Eng* 2010;43:891–906.

529 [6] Meyer S, Lynch R. Microseismic monitoring and short term hazard assessments in underground  
530 coal mines. *Recent Advances in Rock Engineering (RARE 2016)*, Atlantis Press; 2016, p. 446–9.

531 [7] Cheng G, Tang C, Li L, Chuai X, Yang T, Wei L. Micro-fracture Precursors of Water Flow  
532 Channels Induced by Coal Mining: A Case Study. *Mine Water Environ* 2021;40:398–414.

533 [8] Luxbacher K, Westman E, Swanson P, Karfakis M. Three-dimensional time-lapse velocity  
534 tomography of an underground longwall panel. *Int J Rock Mech Min Sci* 2008;45:478–85.

535 [9] Cao W, Durucan S, Cai W, Shi J-Q, Korre A. A physics-based probabilistic forecasting  
536 methodology for hazardous microseismicity associated with longwall coal mining. *Int J Coal Geol*  
537 2020;232:103627.

538 [10] Leśniak A, Ślędz E, Mirek K. Detailed Recognition of Seismogenic Structures Activated during  
539 Underground Coal Mining: A Case Study from Bobrek Mine, Poland. *Energies* 2020;13:4622.

540 [11] Swanson P, Boltz MS, Chambers D. *Seismic Monitoring Strategies for Deep Longwall Coal Mines*.  
541 National Institute for Occupational Safety and Health; 2016.

542 [12] Hartog AH. *An introduction to distributed optical fibre sensors*. CRC press; 2017.

543 [13] Webster P, Wall J, Perkins C, Molenaar M. *Micro-Seismic Detection using Distributed Acoustic*  
544 *Sensing*. Seg Technical Program Expanded Abstracts 2013. <https://doi.org/10.1190/SEGAM2013-0182.1>.

- 545 [14] Lindsey NJ, Martin ER, Dreger DS, Freifeld B, Cole S, James SR, et al. Fiber-optic network  
546 observations of earthquake wavefields. *Geophys Res Lett* 2017;44:11–792.
- 547 [15] Spica ZJ, Perton M, Martin ER, Beroza GC, Biondi B. Urban Seismic Site Characterization by  
548 Fiber-Optic Seismology. *J Geophys Res [Solid Earth]* 2020;125:1251.
- 549 [16] Lindsey NJ, Martin ER. Fiber-optic seismology. *Annual Review of Earth and Planetary*  
550 *2021;49:303–36.*
- 551 [17] Cunningham E, Lord N, Fratta D, Chavarria A, Thurber C, Wang H. Three-dimensional distributed  
552 acoustic sensing at the Sanford Underground Research Facility. *Geophysics* 2023;88:WC209–20.
- 553 [18] Zeng X, Wang HF, Lord N, Fratta D, Coleman T. Field Trial of Distributed Acoustic Sensing in an  
554 Active Room-and-Pillar Mine. In: Yingping Li, Martin Karrenbach, Jonathan B. Ajo-Franklin, editor.  
555 *Distributed Acoustic Sensing in Geophysics: Methods and Applications*, Wiley; 2021, p. 65–79.
- 556 [19] du Toit HJ, Goldswain G, Olivier G. Can DAS be used to monitor mining induced seismicity? *Int J*  
557 *Rock Mech Min Sci* 2022;155:105127.
- 558 [20] Luo X, Duan Y. A field trial of distributed optic fiber sensing technique for longwall caving  
559 mapping. *Rockburst and Seismicity in Mines*, Society for Mining Metallurgy and Exploration; 2022.
- 560 [21] Chambers D, Shragge J. Seismoacoustic Monitoring of a Longwall Face Using Distributed Acoustic  
561 Sensing. *Bull Seismol Soc Am* 2023;113:1652–63.
- 562 [22] Peng SS. *Longwall Mining*, 3rd Edition. CRC Press; 2019.
- 563 [23] Karacan C. Modeling and prediction of ventilation methane emissions of U.S. longwall mines using  
564 supervised artificial neural networks. *Int J Coal Geol* 2008;73:371–87.
- 565 [24] Einicke G, Ralston J, Hargrave C, Reid D, Hainsworth D. The Application of Smoothing within  
566 Longwall Mine Navigation. *Proceedings of the International Global Navigation Satellite Systems Society*  
567 *IGNSS Symposium*, 2009, p. 1–3.
- 568 [25] Mark C. Coal bursts in the deep longwall mines of the United States. *International Journal of Coal*  
569 *Science & Technology* 2016;3:1–9.
- 570 [26] Wang HF, Zeng X, Miller DE, Fratta D, Feigl KL, Thurber CH, et al. Ground motion response to  
571 an ML 4.3 earthquake using co-located distributed acoustic sensing and seismometer arrays. *Geophys J Int*  
572 *2018;213:2020–36.*

- 573 [27] Lindsey NJ, Rademacher H, Ajo-Franklin JB. On the broadband instrument response of fiber-optic  
574 DAS arrays. *J Geophys Res [Solid Earth]* 2020;125. <https://doi.org/10.1029/2019jb018145>.
- 575 [28] Dean T, Cuny T, Hartog AH. The effect of gauge length on axially incident P-waves measured using  
576 fibre optic distributed vibration sensing. *Geophys Prospect* 2017;65:184–93.
- 577 [29] Martin ER, Lindsey NJ, Ajo-Franklin JB, Biondi BL. Introduction to Interferometry of Fiber-Optic  
578 Strain Measurements. In: Yingping Li, Martin Karrenbach, Jonathan B. Ajo-Franklin, editor. *Distributed  
579 Acoustic Sensing in Geophysics: Methods and Applications*, Wiley Online Library; 2021, p. 111–29.
- 580 [30] Virtanen P, Gommers R, Oliphant TE, Haberland M, Reddy T, Cournapeau D, et al. SciPy 1.0:  
581 fundamental algorithms for scientific computing in Python. *Nat Methods* 2020.  
582 <https://doi.org/10.1038/s41592-019-0686-2>.
- 583 [31] Verdon JP, Horne SA, Clarke A, Stork AL, Baird AF, Kendall J-M. Microseismic monitoring using  
584 a fiber-optic distributed acoustic sensor array. *Geophysics* 2020;85:KS89–99.
- 585 [32] Benioff H. A linear strain seismograph. *Bull Seismol Soc Am* 1935;25:283–309.
- 586 [33] Staněk F, Jin G, Simmons J. Fracture Imaging Using DAS-Recorded Microseismic Events. *Front  
587 Earth Sci Chin* 2022;10. <https://doi.org/10.3389/feart.2022.907749>.
- 588 [34] Van Dyke MA, Su WH, Wickline J. Evaluation of seismic potential in a longwall mine with massive  
589 sandstone roof under deep overburden. *Int J Min Sci Technol* 2018;28:115–9.
- 590 [35] Harmon N, Rychert CA, Davis J, Brambilla G, Buffet W, Chichester B, et al. Surface deployment  
591 of DAS systems: Coupling strategies and comparisons to geophone data. *Near Surf Geophys* 2022;20:465–  
592 77.
- 593 [36] Liu TY, Meng XJ, Wang FQ, Li RC, Hou MY, Wang ZW, et al. Fibre optic sensor for coal mine  
594 combustion detection. *Mining Goes Digital*, London: CRC Press; 2019, p. 647–52.
- 595 [37] Lynch R. Microseismic Monitoring of Underground Coal Mines: Objectives, Warnings and Sensor  
596 Array Design. *Proceedings of the 18th Coal Operators' Conference*, ro.uow.edu.au; 2018, p. 31–8.
- 597 [38] Gal M, Reading AM, Rawlinson N, Schulte-Pelkum V. Matched field processing of three -  
598 component seismic array data applied to Rayleigh and love microseisms. *J Geophys Res [Solid Earth]*  
599 2018;123:6871–89.

- 600 [39] Boltz MS, Chambers DJ, Hanson DR. Evaluating Seismicity at Underground Coal Mines Using  
601 Temporary Surface Geophone Deployments. 52nd US Rock Mechanics/Geomechanics Symposium,  
602 American Rock Mechanics Association; 2018.
- 603 [40] Correa J, Egorov A, Tertyshnikov K, Bona A, Pevzner R, Dean T, et al. Analysis of signal to noise  
604 and directivity characteristics of DAS VSP at near and far offsets — A CO2CRC Otway Project data  
605 example. *Lead Edge* 2017;36:994a1–7.
- 606 [41] Gray I, Gibbons T. Longwall behaviour in massive strata. Proceedings of the 2020 Coal Operators’  
607 Conference, University of Wollongong; 2020, p. 47–13.
- 608 [42] Iannacchione AT, Tadolini SC. Occurrence, predication, and control of coal burst events in the U.S.  
609 *International Journal of Mining Science and Technology* 2016;26:39–46.
- 610 [43] Rice GS. Bumps in coal mines—theories of causes and suggested means of prevention or of  
611 minimizing effects. *Transactions of the American Institute of Mining and Metallurgical Engineers*  
612 1936;36:3–23.
- 613 [44] Zafar S, Hedayat A, Moradian O. Evaluation of Crack Initiation and Damage in Intact Barre Granite  
614 Rocks Using Acoustic Emission. *Geo-Congress 2020* 2020:399–408.
- 615 [45] Yang J, Shragge J. Long-term ambient seismic interferometry for constraining seasonal subsurface  
616 velocity variations in urban settings: a distributed acoustic sensing (DAS) case study. *Geophys J Int*  
617 2023;234:1973–84.
- 618 [46] Luo B, Jin G, Stanek F. Near-field strain in distributed acoustic sensing-based microseismic  
619 observation. *Geophysics* 2021;86:49–60.
- 620 [47] Jin G, Roy B. Hydraulic-fracture geometry characterization using low-frequency DAS signal. *Lead*  
621 *Edge* 2017;36:975–80.
- 622 [48] Titov A, Dadi S, Galban G, Norbeck J, Almasoodi M, Pelton K, et al. Optimization of enhanced  
623 geothermal system operations using distributed fiber optic sensing and offset pressure monitoring.  
624 Proceedings of the SPE hydraulic fracturing technology conference and exhibition, 2024.  
625 <https://doi.org/10.2118/217810-MS>.
- 626 [49] Chambers D, Jin G, Tourei A, Issah AHS, Lellouch A, Martin E, et al. DASCore: A Python library  
627 for distributed fiber optic sensing. *Seismica* 2024;3. <https://doi.org/10.26443/seismica.v3i2.1184>.

628

**12 Appendix A: DAS IU Configuration**

629

Table 1 DAS IU configuration for each experiment. Abbreviations used: PW is pulse width, GL is gauge

630

length, FL is fiber length, dt is time sampling interval, and dx is spatial sampling interval (also called channel

631

spacing)

Experiment	Manufacturer	Model	Pulse Width (m)	Gauge Length (m)	Fiber Length (km)	dt (ms)	dx (m)
Gateroad (Section 3)	Terra15	Treble	5.7	5.7	7.1	0.5	5.7
Vertical Surface Borehole (Section 4)	Terra15	Treble	7.4	7.4	1.5	0.35	2.5
Directional Surface Borehole (Section 4)	Terra15	Treble +	9.8	9.8	1.4	0.15	4.9
In-mine Borehole (Section 5)	Terra15	Treble	4.1	8.1	0.5	0.13	1.6
Seismoacoustic (Section 6)	Terra15	Treble	10.6	21.2	3.0	0.12	5.7
Cable Tray (Section 6)	Terra15	Treble	5.7	11.4	1.3	0.2	2.5
Support Can (Section 7)	Terra15	Treble	5.7	11.4	0.8	0.17	2.45

632

633